Geol. Mag. **156** (*4*), *2019, pp. 745–758* © *Cambridge University Press 2018*
doi:10.1017/S0016756818000171

Rifting in SW China: structural and sedimentary investigation of the initial crustal response to emplacement of the Permian Emeishan LIP

YU WANG*†, INGRID UKSTINS PEATE‡, ZHAOHUA LUO*, SHUZHI WANG*, LILU CHENG§, JINHUA HAO* & YE WANG*

*Institute of Earth Sciences, China University of Geosciences, Beijing 100083, China
‡Earth and Environmental Sciences, 115 Trowbridge Hall, University of Iowa, Iowa City, Iowa 52242, USA
§Earth Observatory of Singapore, 50 Nanyang Avenue, Singapore 639798, Singapore

(*Received* 18 November 2016; *accepted* 5 February 2018; *first published online* 21 March 2018)

Abstract – Detailed structural, volcanic, and sedimentary investigations of the crustal response to the emplacement of the Middle–Late Permian Emeishan large igneous province show that a rifting system developed prior to the main stage of flood basalt eruptions, in the form of sedimentary breccias, clastic sedimentary deposits and mafic hydromagmatic units. Detrital zircon grains from sandstones yield ~750–800 Ma LA-ICP-MS $^{206}Pb/^{238}U$ age clusters, showing that material was sourced from the Yangtze crystalline basement. Gabbros and pegmatites intruded along the normal faults of the rift system yield zircon ages of 264–260 Ma, and thus constrain the timing of rifting. N–S-trending rift zones developed along the western flank of the Pan-Xi palaeo-uplift, with NE–SW- and NNE–SSW-trending rifts on the eastern side and along the western and eastern margins of the Yangtze Block. The rifting progressed in pulses, with an initial phase of normal faulting followed by rapid deposition of breccias. Later there was lower-energy deposition of sandstone, with accompanying rhyolitic eruptions. This was followed by low-energy sedimentation of mudstones and dolomites, with accompanying hydromagmatic deposits. Rift system formation was constrained by a combination of far- and near-field tectonic stresses due to plate motions and lithospheric interaction with initial Emeishan volcanism.

Keywords: Emeishan LIP, SW China, initial lithospheric response, rifting, Permian, pulses of rift processes, far-field and near-field stresses

1. Introduction

The initial response of the lithosphere to initiation of flood volcanism is much debated (Campbell & Griffiths, 1990; Griffiths & Campbell, 1991; Coffin & Eldholm, 1994; Farnetani and Richards, 1994; Peterman and Sims, 1998; Corti *et al.* 2003; DePaolo & Manga, 2003; Elkins-Tanton, 2007; Corti, 2009; Cloetingh *et al.* 2013). Several hypotheses have been proposed for lithosphere response, such as rifting (Ziegler, 1992; Ziegler & Cloetingh, 2004), mantle plume-generated uplift (DePaolo & Manga, 2003; Campbell, 2005, 2007; Pierce & Morgan, 2009), and intraplate magmatism in an oceanic or continental setting (Storey, Alabaster & Pankhurst, 1992; Silver *et al.* 2006). These have focused mainly on magmatism and the mechanisms of crustal extension (Sachau & Koehn, 2010). The tectonic setting of the volcanic eruptions, such as a continental interior or margin, is also an important factor. In recent years, continental large igneous provinces (LIPs) and flood basalts (Lassiter & DePaolo, 1997; Bryan & Ernst, 2008 and references therein; Ernst, 2014) have provided a focus for these studies. Ziegler (1992) suggested that two kinds of stress control the eruptive activity, namely far-field and near-field. Magmas propagate through sometimes thick lithosphere before erupting, and near-field stress due to magma upwelling has been emphasized in mantle-plume (e.g. Campbell, 2005, 2007) and rift system settings (e.g. Ziegler & Cloetingh, 2004). However, on a regional scale, intraplate volcanic eruptions are not just controlled by magma upwelling, but also by the tectonic setting and state of stress prior to emplacement. It is thus likely that some combination of the far-field tectonic stress (due to plate motion and plate subduction) and the near-field stress (due to the upwelling of magma) controls LIP formation, including the timing, tectonic position, and the nature of the initial response structure, whether it be an extensional rift (White & McKenzie, 1989) or domal uplift (Griffiths & Campbell, 1991).

The Emeishan LIP formed during the Middle to Late Permian (Figs 1, 2), and is used here as a case study to examine the tectonic relationships of near-field stress from the impact of a upwelling mantle and far-field stress related to plate motions and asthenospheric flow. The Emeishan LIP covers 250,000 km^2, and is distributed in the western Yangtze Block and along its

†Author for correspondence: wangy@cugb.edu.cn

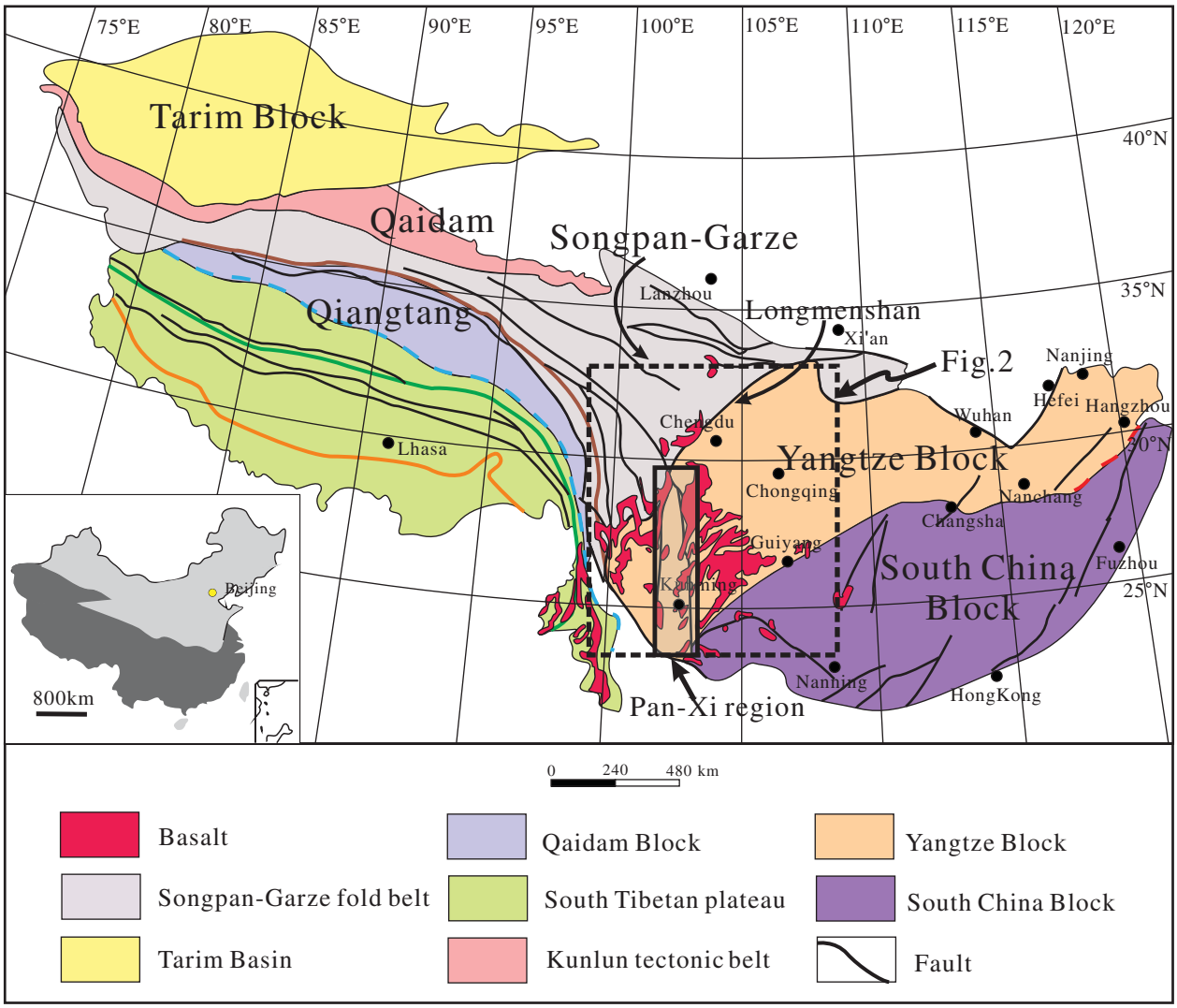

Figure 1. (Colour online) Tectonic setting of the Yangtze Block and the distribution of the Emeishan LIP (simplified from Ren *et al.* 1999). The Tibetan Plateau, southeast China, and the western China tectonic units surround the Yangtze Block. The Pan-Xi (Panzhihua–Xichang) palaeo-uplift zone is also shown. The location of Figure 2 is shown.

southeastern margin (Fig. 1). Prior to eruption there was a long-lived, stable shallow continental sea which existed since the late Proterozoic (Sheng & Jin, 1994). Then sedimentary environment transited to deposition of thick back-arc Triassic sediments, Middle–Late Triassic deformation on the western side of the Pan-Xi region, and thin paralic, coal-bearing and shallow marine successions on the east (Xiao *et al.* 2008; Yang *et al.* 2012). The links between depositional facies changes, volcanism and tectonic response to LIP emplacement have not been explored in detail.

Previous studies have shown that Emeishan LIP eruptions took place in the Middle to Late Permian (Ali *et al.* 2005; Sun *et al.* 2010; Shellnutt, 2014; Li *et al.* 2015), and it has been proposed that they were associated with *c.* 1 km of pre-volcanic domal uplift (He *et al.* 2003). However, several authors have disputed this interpretation (Ukstins Peate & Bryan, 2008, 2009; Ali, Fitton & Herzberg, 2010; Sun *et al.* 2010; Ukstins Peate *et al.* 2011; Shellnutt, 2014; Wang *et al.* 2014, 2015; Jerram *et al.* 2016). Shellnutt (2014) actually did not specifically support domal uplift and he gave an alternative interpretation that the centre of the Yangtze Craton was a topographic high and that domal uplift probably did not occur. Sun *et al.* (2010) show that immediately preceding volcanism, the Maokou Formation directly underlying the Emeishan volcanics experienced rapid subsidence, not uplift, and they also clearly demonstrate that many of the critical Maokou Formation – Emeishan volcanic contacts were misinterpreted, and are actually tectonic juxtapositions, not erosional unconformities. Furthermore, Ukstins Peate & Bryan (2008, 2009) demonstrated that the initial phase of volcanism was hydromagmatic, and occurred at sea level through a stable carbonate platform. However, the pre-existing and syn-volcanic tectonic evolution of the Emeishan is not well constrained, although previous work has discussed some important features. Sun *et al.* (2010) identified submarine slumping of carbonate deposits followed by crustal collapse prior to volcanism, based on sedimentation and palaeobiology on the western side of the Pan-Xi region (Yanyuan

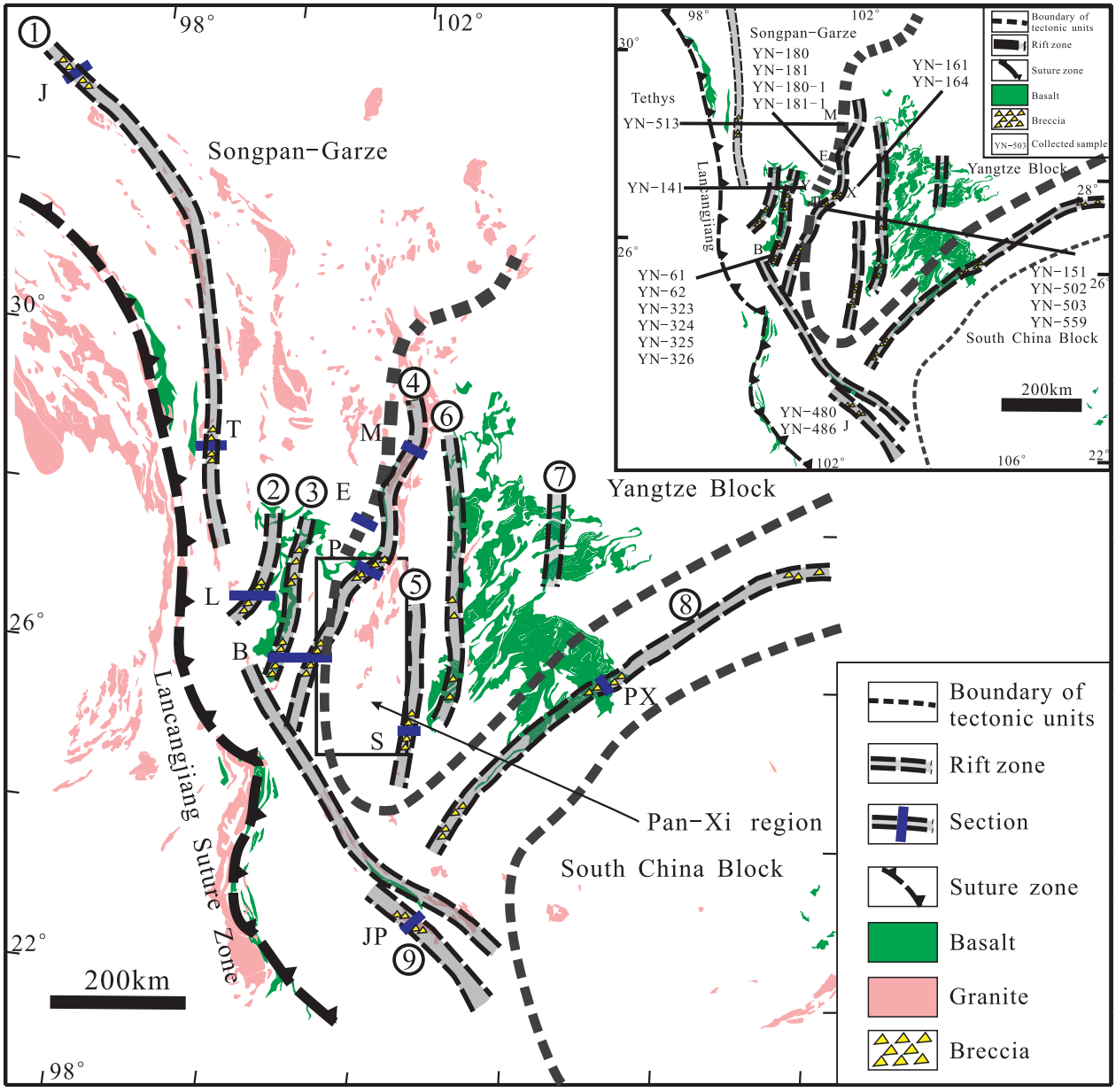

Figure 2. (Colour online) Distribution of the rift zones in the Yangtze Block and its surroundings. The circled numbers are as follows: 1 = Jinsha rift zone, 2 = Lijiang–Wenhua rift zone, 3–4 = Binchuan–Pingchuan rift zone, 4 = Ertan rift zone, 5 = Songming rift zone, 6 = Qiaojia rift zone, 7 = Hezhang rift zone, 8 = Panxian rift zone, 9 = Jinping rift zone. Capital letters show the positions of the detailed cross-sections presented in Figures 3 and 6: T – Tuoding, J – Jinsha, M – Muli, E – Ertan, B – Binchuan, P – Pingchuan, S – Songming, JP – Jinping, PX – Panxian. The present configuration of the rifts is shown. Inset shows sampled sites for sandstone, tuff, gabbro and pegmatite; capital letters show the positions of the collected samples presented in this study.

region). Wignall *et al.* (2009) identified a rift zone on the eastern margin of the province, and prior work also identified a palaeo-rift system in the Pan-Xi region (e.g. Zhang, Luo & Yang, 1988; Luo *et al.* 2001). It is possible that the ELIP is reactivating a Neoproterozoic rift as the Kangdian basalts erupted in the same area (cf. Li *et al.* 2002; Munteanu *et al.*, 2013; Shellnutt *et al.* 2015). Structurally heterogeneity is thought to be an important factor for the location of rifting (Vauchez, Barruol & Tommasi, 1997; Courtillot *et al.* 1999; Buiter & Torsvik, 2014).

For this study, detailed field structural and sedimentologic investigations are used to quantify the location and timing of rift zones formed prior to Emeishan flood volcanism. Based on analysis of detrital and magmatic zircon LA-ICP-MS (laser ablation inductively coupled plasma mass spectrometer) dating to constrain timing of tectonism, we reinterpret the tectonic setting of pre-eruption structural features in terms of the far-field stress due to plate motions and the near-field stress within the plate interior due to lithospheric interaction with mantle emplacement.

2. Tectonic setting and geological features

2.a. Tectonic setting

The Yangtze craton separated from the Gondwana supercontinent during the Cambrian and moved towards

Palaeoasia together with the Tarim and Siberian plates (Huang, Zhou & Zhu, 2008). Until *c*. 280–270 Ma, the Palaeo-Tethys oceanic plate was being subducted under the western margin of the Yangtze Block, forming the Lancangjiang subduction zone (Jian *et al*, 2009; Yang *et al.* 2012; Wang *et al.* 2015). The west Kunlun oceanic plate was also being subducted northwards under the Kunlun–Qinling belt, resulting in the closure of the eastern Palaeo-Tethys Ocean (Wang *et al.* 2015). The Pan-Xi region is a 30 km wide tectonic belt (Wang *et al.* 2014), and its eastern and western sides exhibit similar records of deformation and sedimentation prior to the Late Permian. Along the N–S-trending Pan-Xi region, Proterozoic metamorphic rocks and early Palaeozoic sediment units are exposed, as well as 800–750 Ma granitic intrusions and volcanic eruptions. Similar rocks are also exposed in other uplifted blocks and orogenic belts in SW China. During the early Palaeozoic, the Yangtze Block was dominated by shallow marine to subaerial sedimentation (Liang, Nie & Song, 1994; Jin, Wardlaw & Wang, 1998; Qin, Chen & Tian, 1999; Jin & Sheng, 2000). In the Early Permian, the coal-bearing sediments of the Liangshan Formation were followed by the Qixia and Maokou marine sediments. Prior to the Emeishan LIP eruptions, the Yangtze Block formed a stable craton with northwards plate motion (Huang, Zhou & Zhu, 2008; Wang *et al.* 2015). Emeishan LIP eruptions covered a large area of SW China during the Middle to Late Permian (Figs 1, 2).

2.b. Regional distribution and geological features of the N–S-trending rift zones

We have identified widespread rift features based on detailed field studies (Fig. 2). Rifts have significantly thicker lava successions than outlying areas, and variable sedimentation suggesting accommodation space and deeper-marine environments with intertrappean sediments. These extensional structures represent the initial response of the continental lithosphere of the Yangtze Block prior to the emplacement of the Emeishan LIP in the Middle to Late Permian. Along the western side of the Pan-Xi palaeo-uplift, grabens are N–S-trending, but on the southeastern side of the Yangtze Block, the Panxian–Wujiang zone trends NE–SW. Gabbro dykes and ultramafic sheets, common in the Pan-Xi region, also run parallel to rift system faults (Fig. 3). Many of these intrusive bodies cut the Middle Permian Maokou Formation (Fig. 3), and appear to be emplaced along faults.

3. Sedimentary profiles

We have constructed eight detailed stratigraphic sections based on field studies of sedimentary profiles and structural features. From west to east, the composite profiles are Jinsha, Lijiang–Wenhua, Binchuan, Pingchuan, Muli–Ertan, Jinping, Qiaojia–Songming and Panxian–Wujiang sections (Fig. 2).

3.a. Kuangshanliangzi section, Pingchuan (27° 37′ 25″ N, 101° 53′ 18″ E)

The section near Pingchuan exposes Carboniferous–Permian limestones and sandstones. These are overlain by Middle to Upper Permian Emeishan basaltic lavas (Figs 3–5). A limestone breccia extends along this N–S-trending belt, and beneath this are Early Permian Liangshan Formation coal-bearing layers, which lie on Carboniferous dolomite and limestone (Figs 4, 5). In the breccias, limestone fragments are angular and resemble local wall-rocks. Basal deposits are composed of imbricated blocks of limestone sourced from the Carboniferous dolomite, and the Permian coal-bearing Liangshan and Maokou formations with siliceous sandstone fragments. Clast rotation, sub-faults oriented parallel to the main rift bounding faults, and breccia lithologies sourced from the surrounding stratigraphic sections found in basin walls all suggest these clastic deposits are locally sourced from rift basin walls. Above the breccia, thinly laminated limestones and dolomites are intercalated with reworked clastic deposits with lithologies similar to underlying breccias (Figs 3, 4). They are found within the uppermost strata close to the top of the Maokou Formation. Up-section, the clastic deposits continue to fine. Notably, however, the uppermost sandstones are coarse- to fine-grained angular packstones made up of variable amounts of quartz grains (*c.* 30–80 %), carbonate clasts (both limestone and dolomite, up to 90 %), plus minor FeS_2, biotite, pyroxene and rare volcanic fragments. Overlying the uppermost fine-grained sandstone is the first Emeishan basalt. In this section, there are no basaltic tuffs or hydromagmatic deposits within the sedimentary layers that directly underlie the Emeishan lavas.

3.b. Ertan section (26° 49′ 15″ N, 101° 46′ 32″ E)

Along the Ertan section, a thin breccia (∼1 m thick) associated with a normal fault is exposed (Fig. 3). It has a red/grey colour and comprises blocks of Maokou limestone (Fig. 4i, j). The oriented clasts indicate extensional features, and are aligned sub-parallel to the normal fault surface. The footwall of the normal fault brings up the Middle Permian Maokou Formation and Early Permian Qixia Formation; these formations dip 60–70° to the west/northwest. The fault breccias comprise limestone and rounded blocks of dolomite, granite and basement schist; microfaults can be seen in the pebbles. The parallel orientation of the pebbles, and the sliding and rotation of very small fragments of limestone are consistent with features of syn-deformation sedimentation. Overlying the breccias are two layers of sandstone, a coarse-grained quartz-rich packstone ∼4 m thick (Fig. 5b) and a fine-grained quartz- and calcite-bearing sandstone with calcite cement that is ∼5 m thick (Fig. 5c). The siliciclastic deposits are dominantly clast-supported, and contain quartz, feldspar and minor hornblende (Fig. 5d). The sandstone layers are capped by 20 m of green claystone and red

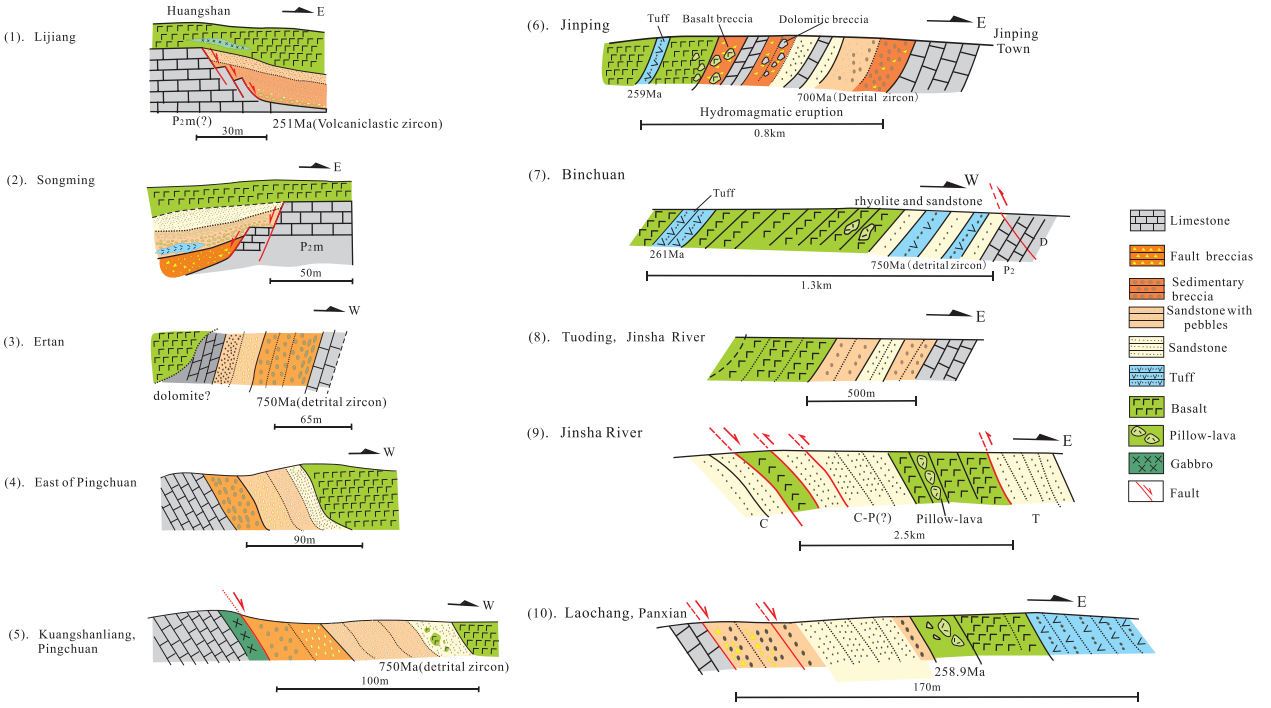

Figure 3. (Colour online) Cross-sections showing the structures and sedimentary units in the area. The locations of these sections are shown in Figure 2. Age data are from this study.

dolomite which is overlain by a ~30 m thick dolomite, all of which sits beneath basalts and basalt-bearing clastic deposits that include a thin layer (~ 3 m) of accretionary and armoured lapilli-bearing mafic volcaniclastic deposits (MVDs) (Fig. 5e).

3.c. Binchuan rhyolite section (from 25° 40′ 32″ N, 100° 21′ 01″ E to 25° 40′ 40″ N, 100° 21′ 20″ E)

The lowermost part of the Binchuan section exposes the Middle Permian Maokou Formation and Devonian limestones (Qingshan Formation) (Fig. 3). Above them (towards the east), there are sandstones, rhyolites and basalt. The sandstone is fine-grained and quartz-rich, and is overlain by a 120 m thick rhyolite with quartz phenocrysts. The rhyolite and sandstone layers are intercalated and have similar dips to the east with an angle of 40–45°.

3.d. Jinping section (22° 44′ 51″ N, 103° 10′ 40″ E)

The Jinping section is on the south side of the Red River sinistral strike-slip fault system near Vietnam. Deposits in this section dip 45–50° towards the WNW. The section exposes the Maokou limestone which is overlain by *c.* 50 m of intercalated MVDs including scoria beds (Fig. 4g, h). These units range upwards from *c.* 80 to 90 % brecciated carbonate in a matrix to predominantly mafic clasts, carbonate clasts and feldspar grains, with calcite cement. These hydromagmatic deposits are all characterized by variable quantities of carbonate materials from the active carbonate platform, and suggest that this phase of volcanism occurred in a shallow marine setting. Above this, the carbonate component becomes less abundant, and deposits transition to ash fall tuffs and volcanic breccias dominated by mafic components. These are followed by the main basaltic eruptions.

3.e. Other localities

The Laochang section (25° 37′ 11″ N, 104° 47′ 02″ E) in the Panxian region trends NE–SW to NE near Wujiang. Within this NE–SW-trending zone, there are, from bottom to top, limestone breccias (20 m), dolomitic breccias (~100 m), sandstones with dolomite clasts (20 m), hydromagmatic deposits (~5 m), basaltic breccias, lavas and tuffs (~20 m) (Fig. 3). The Lijiang (26° 53′ 04″ N, 100° 10′ 46″ E), Wenhua (26° 58′ 07″ N, 100° 22′ 07″ E), Hezhang (26° 54′ 49″ N, 104° 50′ 48″ E) and Qiaojia–Songming (Songming: 25° 20′ 14″ N, 103° 00′ 08″ E) sections share similar features (Fig. 3). At Lijiang, normal faults in the limestone (presumed to be Maokou Formation) are clearly visible, and are overlain by red sandstone and claystones, and volcaniclastic deposits (Fig. 5A), which in turn are overlain by basaltic lavas. In the Songming and Wenhua areas, limestone breccia is at the base of these sections, which begins to display basaltic lithic fragments up-section, and is then topped by tuffaceous sandstones and finally basalt lavas.

3.f. A brief summary

Based on the detailed field stratigraphy and geochronology discussed above, we have compiled a

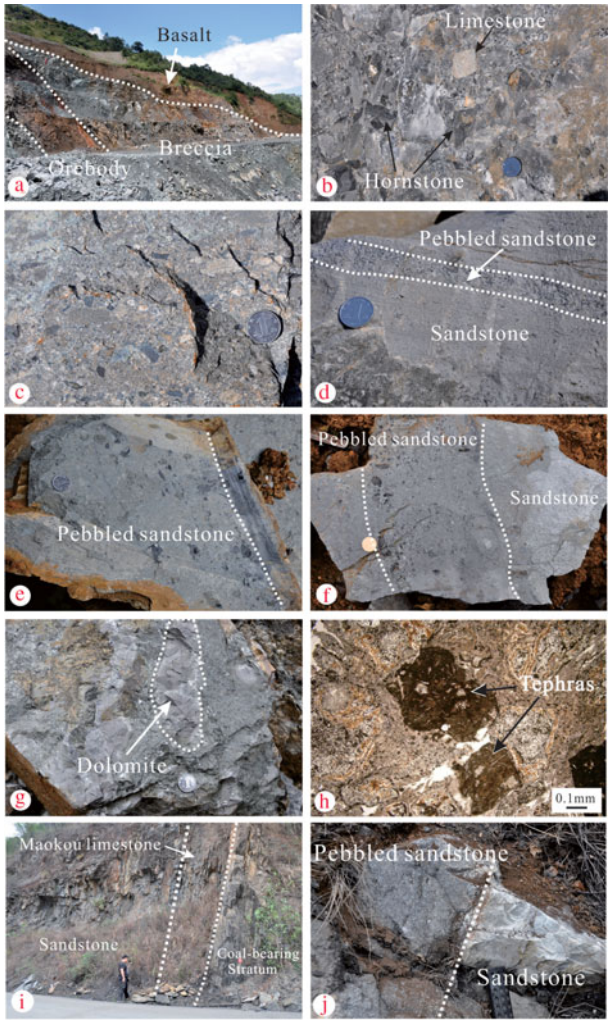

Figure 4. (Colour online) Field photographs and microphotographs of breccia, sandstone and hydromagmatic deposits beneath the Emeishan LIP eruptions. (a) Cross-section of sandstone and breccia, and the contact between sandstone and basalt in the Pingchuan area. (b) Limestone breccia composed of angular clasts in a limestone matrix, from the Pingchuan area. (c) Fine-grained breccia with varied lithic clasts from the Pingchuan area. (d) Sedimentary layers of fine-grained breccia and sandstone in a breccia-bearing sandstone from the Pingchuan area. (e) Limestone breccia-bearing sandstone with thin limestone layers in the Jinping area. (f) Sedimentary sequence from breccia to sandstone in the Jinping area. (g) Hydromagmatic deposits in a matrix of dolomite, Jinping area. (h) Microphotograph showing the volcanic rocks within the dolomite (the thin-section was prepared from the sample shown in (g). (i) Cross-section showing vertical beds of the Permian Maokou limestone and sandstone. (j) Contact between the sandstone and clast-supported packstones, from the locality shown in (i).

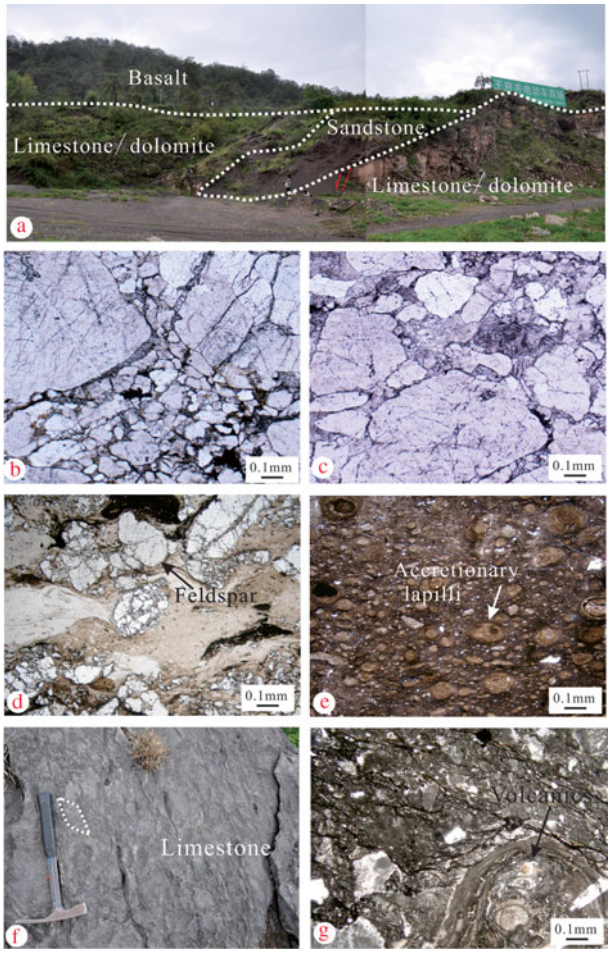

Figure 5. (Colour online) Field photographs and microphotographs of contact between basalt and limestone, and the fault breccias in the Emeishan LIP. (a) Claystone and volcaniclastics are between basalt and Late Permian limestone, west of Lijiang. Note the red-coloured sandstone and volcaniclastics within the contact zone. (b) Coarse-grained quartz-rich packstone (sample YN-180) at Ertan. (c) Quartz- and calcite-bearing sandstone with calcite cement (sample YN-181) at Ertan. (d) Microphotograph of clast-supported packstones, showing syn-depositional deformation that occurred during formation of the fault breccia at Ertan. The rotated and deformed pebbles contain feldspar and quartz, and the matrix is claystone. (e) Mafic volcaniclastic deposits (MVDs) – accretionary lapilli in a surge deposit or airfall tuff at Ertan. (f) Syn-depositional fault breccia at Pingchuan. Both the pebbles and the matrix are limestone, and the pebbles are aligned. (g) Microphotograph showing breccia composed of limestone and volcanic pebbles, at Pingchuan.

composite section representing the rift basin stratigraphy immediately underlying the Emeishan basalts through to the Maokou Formation (Fig. 6). Local erosion and deposition along rift basin margins results in the accumulation of angular, carbonate-bearing breccias which resemble local lithologies. These deposits are fine up-section, transitioning to silicate-bearing sandstones and mudstones. Dolomite deposition re-establishes itself, and the influence of magmatism begins to be observed with the occurrence of hydromagmatic and volcaniclastic deposits. The eruption was through the active carbonate platform and pyroclastic deposits which immediately precede and are intercalated with the lowermost Emeishan basalt lavas.

The Maokou Formation is cut by faults and has different thicknesses on either side of the fault zones, such as along the Qiaojia–Songming zone and in the west of the Pingchuan area. In some places, there are ~50–200 m differences in the thickness of the Maokou Formation on either side of a fault. In the hanging walls of both fault zones deep-water

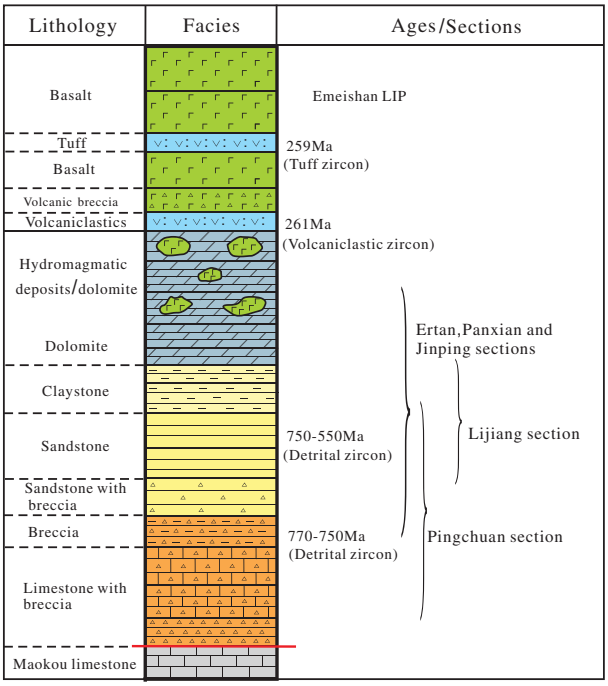

Figure 6. (Colour online) Summary volcanostratigraphic section for the rift zones in the Emeishan LIP. Age data are from this study.

Figure 7. (Colour online) Representative CL images of analysed zircons from sandstone samples YN-61, YN-161, YN-181 and YN-513, collected from Binchuan, Xichang, Ertan and Muli, respectively. Analysis spots are indicated by yellow circles, and calculated $^{206}Pb/^{238}U$ ages are indicated. Other CL images are shown in Data Repository 1 (in Supplementary Material at https://doi.org/10.1017/S0016756818000171).

siliceous sediments, such as chert, can be found. This is an important constraint on the initiation of the rift system, and indicates that the normal faulting did not take place after the Maokou Formation, but was contemporaneous with its deposition. In summary, the deposition of the Maokou Formation was associated with the rifting, and the sedimentary profiles in all the above sections provide a detailed record of the rifting system (Fig. 6).

4. Geochronology analytical methods

4.a. Sample collection and preparation

Twenty samples were collected for U–Pb dating, representing all rock units and tectonic settings considered in this study (Fig. 2 inset; Table 1). Sediments were sampled close to the fault zone in the Pingchuan section (samples YN-502, YN-503 and YN-559), the Ertan section (YN-180, YN-180-1, YN-181 and YN-181-1) and the Jinping section (YN-486). Away from the fault zone, detrital samples were collected from the Binchuan section (samples YN-61, YN-62, YN-323, YN-324, YN-325 and YN-326), as well as a sample from a Triassic sandstone (YN-141). Also sampled were associated volcanic units represented by the Muli tuff (YN-513), the Jinping tuff (YN-480) and three gabbro and pegmatite samples from the area around Pingchuan (YN-151, YN-161 and YN-164).

Zircons were separated using conventional techniques, including heavy liquids and magnetic separation, and were hand-picked under a binocular microscope. Grains were mounted in epoxy discs, polished to half their thickness and photographed in transmitted and reflected light to reveal the internal structures of the zircons. After gold coating, cathodoluminescence (CL) images (Fig. 7; Data Repository 1 in Supplementary Material at https://doi.org/10.1017/S0016756818000171) were obtained to identify internal structures and select potential spots for analysis.

4.b. Determination of U–Pb zircon ages

U–Pb ages were performed by LA-ICP-MS, using two instruments housed at the China University of Geosciences, Wuhan, China, and at the University of Science and Technology of China, Hefei, China, using a ~30 μm diameter spot size and laboratory procedures described by Liu *et al.* (2004). A 91500 zircon was used as an external standard during the age calculations, and was measured every five or six analyses; in addition, the NIST SRM610 standard was analysed twice every 20 analyses of U, Th and Pb. U–Pb ages were calculated using ISOPLOT 3.23 (Ludwig, 2005). Sample descriptions are summarized in Table 1. Analytical data are provided in Data Repository 2 (in Supplementary Material at https://doi.org/10.1017/S0016756818000171), and selected age plots are shown in Figure 8 and in Data Repository 3 (in Supplementary Material at https://doi.org/10.1017/S0016756818000171).

Table 1. Sampled sites, petrologic descriptions and zircon age data in Emeishan LIP area

Sample no.	Location	Petrologic description	Position in the field	$^{206}Pb/^{238}U$ mean age
YN-61	25° 40′ 33″ N, 100° 21′ 03″ E	Sandstone interlayered with rhyolite	Binchuan	Scattered, 454–3027 Ma
YN-62	25° 40′ 33″ N, 100° 21′ 04″ E	Sandstone interlayered with rhyolite	Binchuan	Scattered, 294–3083 Ma
YN-323	25° 40′ 33″ N, 100° 21′ 03″ E	Sandstone	Binchuan	795 ± 41 Ma (n = 29); others scattered, 452–3484 Ma
YN-324	25° 40′ 33″ N, 100° 21′ 03″ E	Sandstone	Binchuan	Scattered, 452–3342 Ma
YN-325	25° 40′ 33″ N, 100° 21′ 03″ E	Sandstone	Binchuan	Scattered, 389–2784 Ma
YN-326	25° 40′ 33″ N, 100° 21′ 03″ E	Sandstone	Binchuan	Scattered, 498–3190 Ma
YN-141	26° 46′ 15″ N, 100° 47′ 15″ E	Triassic sandstone	Yongsheng	Scattered, 266–3149 Ma
YN-151	27° 37′ 25″ N, 101° 53′ 18″ E	Gabbro	Pingchuan	262 ± 4.1 Ma (n = 40)
YN-161	27° 54′ 19″ N, 102° 07′ 30″ E	Gabbro	Xichang	264.6 ± 3.8 Ma (n = 36)
YN-164	27° 54′ 19″ N, 102° 07′ 30″ E	Pegmatite	Xichang	263.5 ± 3.6 Ma (n = 16)
YN-180	26° 49′ 15″ N, 101° 46′ 33″ E	Sandstone	Ertan	740 ± 11 Ma (n = 41)
YN-180-1	26° 49′ 15″ N, 101° 46′ 33″ E	Sandstone (fine grain)	Ertan	755 ± 10 Ma (n = 71)
YN-181	26° 49′ 15″ N, 101° 46′ 33″ E	Sandstone	Ertan	750 ± 10 Ma (n = 38)
YN-181-1	26° 49′ 15″ N, 101° 46′ 33″ E	Sandstone (fine grain)	Ertan	735 ± 12 Ma (n = 47)
YN-480	22° 43′ 48″ N, 103° 09′ 42″ E	Tuff	Jinping	259.4 ± 0.9 Ma (n = 36)
YN-486	22° 44′ 51″ N, 103° 10′ 39″ E	Sandstone	Jinping	742 ± 78 Ma (n = 9)
YN-502	27° 36′ 41″ N, 101° 52′ 46″ E	Conglomerate	Pingchuan	776 ± 4 Ma (n = 54)
YN-503	27° 36′ 41″ N, 101° 52′ 46″ E	Sandstone	Pingchuan	786 ± 16 Ma (n = 57)
YN-559	27° 36′ 48″ N, 101° 52′ 47″ E	Sandstone	Pingchuan	753 ± 14 Ma (n = 73)
YN-513	28° 02′ 39″ N, 101° 28′ 13″ E	Tuff	Muli	258.7 ± 1.6 Ma (n = 106)

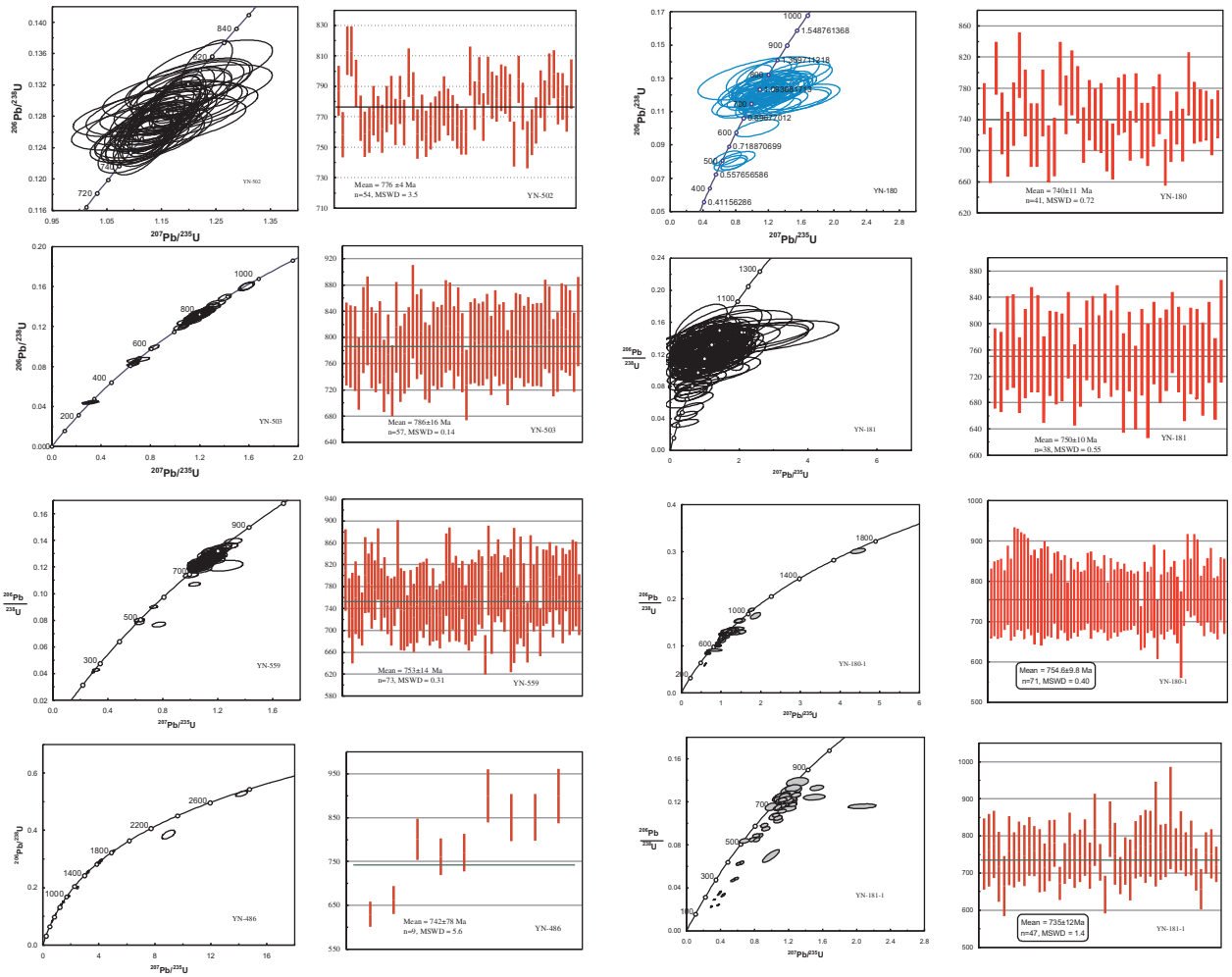

Figure 8. (Colour online) Representative U–Pb concordia diagrams for all rock samples of closed to the normal fault zones. $^{206}Pb/^{238}U$ weighted mean ages of the younger cluster of analyses are also shown. Other U–Pb concordia diagrams are available in Data Repository 3 (in Supplementary Material at https://doi.org/10.1017/S0016756818000171).

5. Analytical results

5.a. CL images of detrital and magmatic zircons

CL images show clear differences between detrital and magmatic zircons (Fig. 7; Data Repository 1, in Supplementary Material at https://doi.org/10.1017/S0016756818000171). The detrital zircons can be divided into sub-types based on their physical shape. In samples YN-502, 503, YN-559, YN-180, 180–1, 181, YN-181-1 and YN-486, euhedral zircons comprise 60–80 % of the total, displaying features such as sharply defined rims, zoned cores and rims. Euhedral zircons are common in the lowermost sedimentary sequence. CL images of detrital zircons from the Ertan section show features indicative of a magmatic origin, with little rounding, no metamorphic alteration, and clear cores and rims. In contrast, rounded zircons without clear rims are found in the Binchuan section; these features are consistent with long-distance or repeated transport of zircon grains. The sample collected from the thick Triassic sedimentary rocks (YN-141) that overlie the basalts contains zircons with complex features (Data Repository 3, in Supplementary Material at https://doi.org/10.1017/S0016756818000171). In the tuffs and gabbros, most zircon grains show features indicative of a magmatic origin. Smaller grains preserve oscillatory zoning from a single growth event, while larger grains contain euhedral, possibly inherited cores overgrown by oscillatory-zoned rims. The appearance of the grains in CL does not vary with Pb or Th concentration, but the loss of U is indicated by white–grey colour.

5.b. Zircon ages of tuffs

Two tuff samples from Jinping (YN-480) and Muli (YN-513) were also dated. The former contains abundant magmatic zircons, and a total of 40 spots were analysed. The U content range is 50–1000 ppm and the Th/U ratios are 0.32–1.97. The analyses cluster from 256 to 264 Ma, among which 36 ages form the group with a $^{206}Pb/^{238}U$ weighted mean age of 259.4 ± 0.9 Ma. For sample YN-513, 128 spots were analysed. The U contents are 50–420 ppm, and the Th/U ratios are 0.4–1.0. The ages vary from 250 to 270 Ma, among which 106 ages form the group with a weighted mean $^{206}Pb/^{238}U$ age of 258.7 ± 1.6 Ma. The ages of other grains do not define clusters, and are either younger than 250 Ma or older than 265 Ma. The two tuff samples show similar age clusters.

5.c. Zircon age of gabbro and pegmatite

In the Pingchuan area, zircons from two gabbro samples (YN-151, YN-161) and one sample of mafic pegmatite dyke (YN-164) yield ages of 265–260 Ma, and the weighted mean $^{206}Pb/^{238}U$ ages for each sample are within error of each other. The ages vary from 250 to 280 Ma; within that range, 15–40 ages in each sample form age clusters with weighted mean $^{206}Pb/^{238}U$ ages of 262 ± 4 Ma, 265 ± 4 Ma and 264 ± 4 Ma, respectively.

5.d. Detrital zircon ages

5.d.1. Kuangshanliangzi section, Pingchuan

Three samples (YN-502, YN-503 and YN-559) were collected from the bottom to the top of the sequence at the Pingchuan section. They range from fine- to coarse-grained angular packstones, containing carbonate clasts, quartz and oxides. For sample YN-502, 73 spots were analysed, yielding U concentrations of 52–2458 ppm, and Th/U ratios of 0.30–1.30. Ages range from 437 to 898 Ma, among which 54 ages define the youngest group with a $^{206}Pb/^{238}U$ weighted mean age of 776 ± 4 Ma. The ages of other grains do not define clusters, and are younger than 700 Ma and older than 800 Ma. For sample YN-503, 75 spots were analysed, yielding U concentrations of 74–615 ppm, and Th/U ratios of 0.30–3.0. Ages range from 273 to 1444 Ma, among which 57 ages define the age clusters with a $^{206}Pb/^{238}U$ weighted mean age of 786 ± 16 Ma. For sample YN-559, 81 spots were analysed, yielding U concentrations of 20–1270 ppm and Th/U ratios of 0.20–2.0. Ages range from 269 to 2485 Ma, among which 73 ages define the age clusters with a $^{206}Pb/^{238}U$ weighted mean age of 753 ± 14 Ma. There are some younger ages between 269–278 Ma for these three samples.

5.d.2. Ertan section

Four samples were collected from the Ertan section, including a coarse-grained quartz-rich sandstone (sample YN-180) that directly overlies the Permian Maokou limestone, and a fine-grained quartz- and calcite-bearing packstone with calcite cement (sample YN-181) that underlies the claystone which covers the sequence. In addition, we examined two more coarse- to fine-grained sandstones (YN-180-1 and YN-181-1). In each sample, 47–99 spots were analysed. The Th contents vary between 50 and 6000 ppm, and U between 60 and 3500 ppm. All four samples yield main ages between 700 and 2900 Ma, the youngest clusters of which form a group with a weighted mean $^{206}Pb/^{238}U$ age of 740 ± 10 Ma (YN-180), 766 ± 12 Ma (YN-181), 755 ± 10 Ma (YN-180-1) and 735 ± 12 Ma (YN-181-1). The ages of other grains do not define clusters, and are younger than 700 Ma and older than 800 Ma. All samples from the Ertan sedimentary profile, regardless of grain size or sedimentary nature, yield similar ages of ∼735–765 Ma; none of the zircon ages are consistent with the ∼260 Ma age of the Emeishan basalt.

5.d.3. Binchuan section

Six samples containing detrital zircons were collected from the base of the Binchuan section. The

sandstones (samples YN-61, YN-62), interlayered with rhyolite, show scattered ages, but include a cluster at 630–720 Ma. For sample YN-61, 58 spots were analysed. The ages range from ~3000 to 540 Ma, among which 24 ages form the youngest group with a weighted mean $^{206}Pb/^{238}U$ age of 630 ± 31 Ma. For sample YN-62, 51 spots were analysed. The ages range from ~3000 to 560 Ma, among which 20 ages form the youngest group with a weighted mean $^{206}Pb/^{238}U$ age of 719 ± 30 Ma. The ages of other grains do not define clusters, and are younger than 600 Ma and older than 800 Ma. None of the zircons was younger than ~260 Ma. The sandstone samples (YN-323, YN-324, YN-325 and YN-326), also interlayered with rhyolite, had several tens of spots analysed, with ages varying from ~400 to 3500 Ma. None of the zircon ages is younger than ~260 Ma. All the samples from this section have different age clusters, regardless of distance to rhyolitic units, thickness, or composition.

5.d.4. Jinping section

In sandstone sample YN-486, 24 spots from 60 zircon grains were analysed and they yielded U concentrations of 91–2545 ppm and Th/U ratios of 0.20–1.20. Ages range from 502 to 2732 Ma, among which nine ages form the youngest group with a weighted mean $^{206}Pb/^{238}U$ age of 742 ± 78 Ma. The ages of other grains do not define clusters, and are younger than 700 Ma and older than 800 Ma. No ages younger than ~260 Ma were obtained. The age data are similar to those of the Pingchuan and Ertan sections, and in all sections the ages of detrital zircons cluster around 750 Ma.

5.d.5. Triassic sandstone at Yongsheng

Sample YN-141 was collected from the Triassic sandstone. A total of 87 spots were analysed. The ages vary from ~3100 to ~600 Ma, among which 54 ages form the youngest group with a weighted mean $^{206}Pb/^{238}U$ age of 620 ± 38 Ma, but with a large MSWD (~2.4). The ages of other grains do not define clusters, and are younger than 600 Ma and older than 800 Ma.

6. Discussion

6.a. Geochronology and timing of volcanism

Whole-rock Ar–Ar dating of Emeishan basalts yields appreciably younger ages than the magnetostratigraphically constrained late Middle Permian age (Ali *et al.* 2004). This appears to reflect thermal resetting during the Mesozoic and Cenozoic (Ali *et al.* 2004). Re-evaluation of previously published Ar–Ar dating studies, combined with these reset ages, led Ali *et al.* to conclude that the overprinting represented three major, *c.* 10 Ma long, tectonic events during the Middle Jurassic (~175 Ma), Late Jurassic – Early Cretaceous (~142 Ma) and Early–Late Cretaceous (~98 Ma), with a shorter middle Eocene episode (~42 Ma). The most likely cause is deformation along the Longmen Shan thrust belt, and potentially final suturing of the North and South China blocks in the Middle Jurassic (Ali *et al.* 2004).

The dominant peak in detrital zircon ages of clastic deposits is between 700 and 800 Ma, with less common ages of ~450–500 Ma. At Ertan, Pingchuan and Jinping, 60–80 % of the zircons are euhedral and show magmatic features in CL. These characteristics indicate that they have not experienced long-distance transport, but were instead derived from proximal sources. The 800–750 Ma ages are typical of those found in adjacent basement rocks of the Yangtze Block (Zhou *et al*. 2002; Geng *et al.* 2007), and indicate derivation from nearby basement rocks during rapid transport and deposition. These sandstones result from rapid sedimentation during the period of normal faulting that marked the end of deposition of the Permian Maokou Formation shallow platform carbonates, and took place before the main phase of basaltic eruptions. They were characterized by rapid deposition, short transport distances and fining-upward sequences which record a change from a single to multiple sources upsection, as demonstrated by the change from a single cluster of U–Pb ages to a more scattered distribution. At sites far from the rift system, such as at Binchuan and in the upper cover of Triassic sandstone, there are no clear clusters of zircon ages. Instead, the ages range from 300 to 2100 Ma, with no correspondence between grain shape and age. Moreover, the grains are rounded to sub-rounded which may represent contributions from multiple source rocks (Dickinson & Gehrels, 2009). The difference in age clusters between samples in this study, together with the degree of grain abrasion, indicates that the transport histories of the individual zircon grains might also be variable. Thus, many of the detrital zircons may be polycyclic (such as ~400–500 Ma; >800 Ma), derived from both proximal and distal areas, although some (~750–800 Ma) may also be from the faulted basement rocks. Finally, the zircon ages from the gabbros and pegmatites represent the timing of volcanic activity. These events occurred at 260–264 Ma within errors (±2 %), and they constrain the onset of extension. The ages of the volcanic deposits in Jinping and Muli that constrain the timing of rifting pre-date ~259 Ma, i.e. prior to the basaltic eruptions.

6.b. Implications of rift system evolution

Sandstone deposition, which records erosion of old crustal materials and near-source infilling of the developing accommodation space in rift systems, took place prior to the initiation of mafic volcanism in the Emeishan (e. g. Binchuan locality). Depositional sequences within rift basins follow the pattern of: (1) initiation of faulting and brecciation; (2) deposition of basal sandstones and breccias, fining upwards; (3)

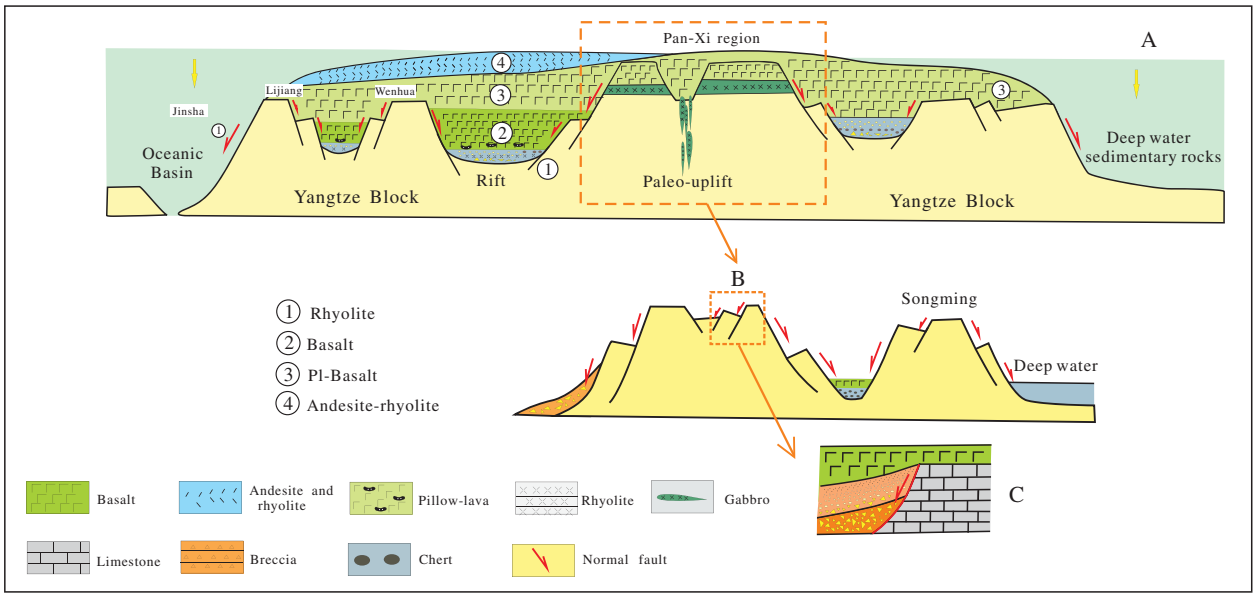

Figure 9. (Colour online) Summary cross-section of the region from west to east, from the initial response to the four stages of volcanic eruption in the region. The inset diagrams show the main two kinds of deformation and the uplift due to faulting in the area.

mudstone or dolomite deposition; (4) hydromagmatic eruptions through shallow carbonate platform environments; and (5) emplacement of basaltic lavas and pillow lavas with associated tephra deposits (Wang *et al.* 2014). The region was already starting to respond to the interaction of crust in near-field tectonic stress with the upwelling mantle prior to initiation of volcanism, and rifting and lithospheric fracturing likely aided in channelling magmatic upwelling (Fig. 9). Palaeobiological observations suggest that the initial stage of the lithospheric response to the upwelling mantle lasts at least 3–5 Ma (Isozaki, Kawahata & Minoshima, 2007; Isozaki, 2009, 2010). Furthermore, there is evidence that pre-volcanic rifting may have progressed sporadically. The variability of clastic sedimentation and cyclicity of coarse clastic deposits transitioning to mudstones and dolomites may reflect slowing of deposition. In addition, the lower Maokou Formation shows the effects of syn-depositional faulting in different thicknesses of the formation on either side of rift zones. This feature is only evident along the rift system itself, such as along the eastern marginal fault of the Pan-Xi region, as well as along the boundary between the Yangtze Block and South China Block. Regionally, from west to east, the N–S-trending rift zones have been well documented, especially along the Binchuan and Pingchuan zones (Figs 2 and 9). In addition, we note that there are high-Ti basalts in the middle–late parts of the volcanic sequence (Xiao *et al.* 2004) in all the LIP areas, but low-Ti basalts only occur in the lower section of the Binchuan rift zone (Xiao *et al.* 2004). This is in contrast to the mantle-plume uplift model, which suggests that low-Ti basalts are found in the core of the uplift and high-Ti basalts occur in the outer zone.

The pre-Emeishan geological history of the Yangtze Block is that of a shallow marine environment, from the Late Carboniferous to Early Permian. Sedimentary sections discussed here, along with new geochronologic ages of tuffs, gabbros and volcaniclastics, clearly show that normal faulting as well as some early eruptions and magmatic intrusions occurred during the period ~264–259 Ma, and this activity all took place prior to the main phase of LIP emplacement. The overall pattern of events involving normal faulting, the channelling of magma along tectonic pathways, eruption of voluminous basaltic flood lavas, and the accompanying crustal depression and sedimentation, indicates that the Emeishan basalt eruption occurred from 260 to 257 Ma as in the range of high-precision dates (Shellnutt, Denyszyn & Mundil, 2012; Zhong *et al.* 2014), but with limited evidence to suggest that ELIP magmatism extended into the Triassic (Shellnutt, Denyszyn & Mundil, 2012).

We infer that the initial crustal response to emplacement of the Emeishan LIP was:

(1) Rift system formation was not continuous and progressed as pulses. Large-scale faults would have acted as channels along which magma could ascend rapidly.

(2) The regional response to initiation of volcanism was transgressive: from the margins to the interior of the Yangtze Block (Fig. 2). Figure 2 shows the location of the rift zones – most are presently oriented N–S and probably reflect an overall E–W extension affecting the South China craton at this time – although the rifts on the west and southeast sides have variable orientations suggesting differences in timing and geodynamic setting.

(3) Detailed stratigraphic and palaeobiology evidence shows that rifting initiated ~5 Ma prior to LIP emplacement. Pre-volcanic tectonic development was dominated by large-scale rift systems and extensional faulting (Fig. 9).

7. Conclusions

The rifting and associated deposits that developed in extensive, pre-volcanic graben systems prior to emplacement of the Emeishan represent the initial response of this intracontinental stable platform to upwelling mantle and incipient emplacement of a LIP. The rift zones occur not only along the continental margins, parallel to pre-existing orogenic belts, but also in the interior of the Yangtze Block. The ages of detrital zircon grains from the sandstones which were deposited in these nascent rift systems show a cluster at 750–800 Ma, and the zircon CL images show that these grains have sharp magmatic features, clearly indicating rapid and short-distance transport of clastic material derived from older crustal exposures developed in the walls of the rifts. Gabbro and pegmatite dykes, intruded along high-angle normal faults forming the rift zone boundaries, yield zircon U–Pb LA-ICP-MS ages of 264–263 Ma, which slightly predates the initial emplacement of the Emeishan volcanics. Equally important, these grabens provided the pathways along which volcanism could be channelled to the surface and thus appear to control the distribution of magma types (lo–Ti, hi–Ti) previously thought to be associated with domal uplift. The initial crustal response to initiation of volcanism progressed as pulses. The formation of the rift system within the relatively stable western Yangtze Block was constrained by the near-field stresses due to the upwelling of mantle, and the far-field tectonic stresses due to plate motions. Together, these systems resulted in crustal–lithospheric extension in the form of linear rifts, which then channelled the magma to the surface to produce the Emeishan LIP.

Acknowledgements. We greatly appreciate the constructive comments and suggestions from the editor of *Geological Magazine*, Prof. S. Hubbard, and reviewers Prof. R. Ernst, Dr G. Shellnutt and an anonymous reviewer. This study was supported by Chinese 973 project (2011CB808901) and the Geological Survey of China. I. Ukstins would like to acknowledge support from NSF EAR-1126728. During the field work, Y. G. Han and H. X. Hei helped in the data collection. Discussions with Profs C. Q. Cao, T. N. Yang, D. P. Yan and S. F. Liu, as well as many other geologists, improved the ideas presented in this article. Z. C. Hu is thanked for the laboratory work on U–Pb dating of the zircons.

Supplementary material

To view supplementary material for this article, please visit https://doi.org/10.1017/S0016756818000171.

References

Ali, J. R., Fitton, J. G. & Herzberg, C. 2010. Emeishan large igneous province (SW China) and the mantle-plume up-doming hypothesis. *Journal of the Geological Society* **167**, 953–9.

Ali, J. R., Lo, C. H., Thompson, G. M. & Song, X. Y. 2004. Emeishan Basalt Ar-Ar overprint ages define several tectonic events that affected the western Yangtze Platform in the Mesozoic and Cenozoic. *Journal of Asian Earth Sciences* **23**, 163–78.

Ali, J. R., Thompson, G. M., Zhou, M.-F. & Song, X. Y. 2005. Emeishan large igneous province, SW China. *Lithos* **79**, 475–89.

Bryan, S. E. & Ernst, R. E. 2008. Revised definition of large igeous provinces (LIPs). *Earth-Science Reviews* **86**, 175–202.

Buiter, S. J. H. & Torsvik, T. H. 2014. A review of Wilson Cycle plate margins: a role for mantle plumes in continental break-up along sutures? *Gondwana Research* **26**, 627–53.

Campbell, I. H. 2005. Large igneous provinces and the mantle plume. *Elements* **1**, 265–9.

Campbell, I. H. 2007. Testing the plume theory. *Chemical Geology* **241**, 153–76.

Campbell, I. H. & Griffiths, R. W. 1990. Implications of mantle plume structure for the evolution of flood Basalts. *Earth and Planetary Science Letters* **99**, 79–93.

Cloetingh, S., Burov, E., Matenco, M., Beekman, F., Roure, F. & Ziegler, P. A. 2013. The Moho in extensional tectonic settings: insights from thermo-mechanical models. *Tectonophysics* **609**, 558–604.

Coffin, M. F. & Eldholm, O. 1994. Large igneous provinces: crustal structure, dimensions and external consequences. *Reviews of Geophysics* **32**, 1–36.

Corti, G. 2009. Continental rift evolution: from rift initiation to incipient break-up in the Main Ethiopian Rift, East Africa. *Earth-Science Reviews* **96**, 1–53.

Corti, G., Bonini, M., Conticelli, S., Innocenti, F., Manetti, P. & Sokoutis, D. 2003. Analogue modelling of continental extension: a review focused on the relations between the patterns of deformation and the presence of magma. *Earth-Science Reviews* **63**, 169–247.

Courtillot, V., Jaupart, C., Manighetti, I., Tapponnier, P. & Besse, J. 1999. On causal links between flood basalts and continental breakup. *Earth and Planetary Science Letters* **166**, 177–95.

DePaolo, D. J. & Manga, M. 2003. Deep origin of hotspots: – the mantle plume model. *Science* **300**, 920–1.

Dickinson, W. R. & Gehrels, G. E. 2009. U-Pb ages of detrital zircons in Jurassic Eolian and associated sandstones of the Colorado Plateau: evidence for transcontinental dispersal and intraregional recycling of sediment. *Geological Society of America Bulletin* **121**, 408–33.

Elkins-Tanton, L. T. 2007. Continental magmatism, volatile recycling, and a heterogeneous mantle caused by lithospheric gravitational instabilities. *Journal of Geophysical Research Planets* **110**, 219–32.

Ernst, R. E. 2014. *Large Igneous Provinces*. Cambridge: Cambridge University Press, 653 pp.

Farnetani, C. G. & Richards, M. A. 1994. Numerical investigations of the mantle plume initiation model for flood basalt events. *Journal Geophysical Research* **99** (B7), 13813–33.

Geng, Y. S., Yang, C. H., Wang, X. S., Ren, L. D., Du, L. L. & Zhou, X. W. 2007. Age of crystalline basement in western margin of Yangtze terrane. *Geological Journal of China Universities* **13**, 429–41 (in Chinese with English abstract).

Griffiths, R. W. & Campbell, I. H. 1991. Interaction of mantle plume heads with the Earth's surface and onset small-scale convection. *Journal of Geophysical Research* **96** (B11), 18275–310.

He, B., Xu, Y. G., Chung, S. L. & Wang, Y. 2003. Sedimentary evidence for a rapid crustal doming before the

eruption of the Emeishan flood basalts. *Earth and Planetary Science Letters* **213**, 389–403.

Huang, B. C., Zhou, X. & Zhu, R.X. 2008. Discussions on Phanerozoic evolution and formation of continental China, based on paleomagnetic studies. *Earth Science Frontiers* **15**, 348–59 (in Chinese with English abstract).

Isozaki, Y. 2009. Illawarra reversal: the fingerprint of a superplume that triggered Pangean breakup and the end-Guadalupian (Permian) mass extinction. *Gondwana Research* **15**, 421–32.

Isozaki, Y. 2010. Reply to the comment by Ali J. R. on 'Illawarra reversal: the fingerprint of a superplume that triggered Pangean breakup and the end-Guadalupian (Permian) mass extinction' by Yukio Isozaki. *Gondwana Research* **17**, 718–20.

Isozaki, Y., Kawahata, H. & Minoshima, K. 2007. The Capitanian (Permian) Kamura cooling event: the beginning of the Paleozoic–Mesozoic transition. *Palaeoworld* **16**, 16–30.

Jerram, D. A., Widdowson, M., Wignall, P. B., Sun, Y. D., Lai, X. Y., Bond, D. P. G. & Torsvik, T. H. 2016. Submarine palaeoenvironments during Emeishan flood basalt volcanism, SW China: implications for plume–lithosphere interaction during the Capitanian, Middle Permian ('end Guadalupian') extinction event. *Palaeogeography, Palaeoclimatology, Palaeoecology* **441**, 65–73.

Jian, P., Liu, D. Y., Kröner, A., Zhang, Q., Wang, Y. Z., Sun, X. M. & Zhang, W. 2009. Devonian to Permian plate tectonic cycle of the Paleo-Tethys Orogen in southwest China (II): insights from zircon ages of ophiolites, arc/back-arc assemblages and within-plate igneous rocks and generation of the Emeishan CFB province. *Lithos*,**113**, 767–84.

Jin, Y. & Sheng, Q. 2000. The Permian of China and its interregional correlation. In *Permo–Triassic Evolution of Tethys and Western Circum-Pacific* (eds H. F. Yin, J. M. Dickins, G. R. Shi & J. N. Tong), pp. 71–98. Amsterdam: Elsevier.

Jin, Y., Wardlaw, B. R. & Wang, Y. 1998. *Permian Stratigraphy, Environments and Resources, vol. 2: Palaeoworld*. Nanjing: Nanjing University Press.

Lassiter, J. C. & DePaolo, D. J. 1997. Plume/lithosphere interaction in the generation of continental and oceanic flood basalts: chemical and isotopic constraints. In *Large Igneous Provinces: Continental, Oceanic, and Planetary Flood Volcanism* (eds J. J. Mahoney and M. F. Coffin), pp. 335–55. The American Geophysical Union, Geophysical Monograph no. 100.

Li, X.-H., Li, Z.-X., Zhou, H., Liu, Y. & Kinny, P. D. 2002. U-Pb zircon geochronology, geochemistry and Nd isotopic study of Neoproterozoic bimodal volcanic rocks in the Kangdian rift of South China: implications for the initial rifting of Rodinia. *Precambrian Research* **113**, 135–54.

Li, H. B., Zhang, Z. C., Ernst, R., Lu, L. S., Santosh, M., Zhang, D. Y. & Cheng, Z. G. 2015. Giant radiating mafic dyke swarm of the Emeishan Large Igneous Province: identifying the mantle plume centre. *Terra Nova* **27**, 247–57.

Liang, D. Y., Nie, Z. T. & Song, Z. M. 1994. Extensional Dongwu movement in western margin of Yangtze region. *Earth Science Journal of China University of Geosciences* **19**, 443–53 (in Chinese with English abstract).

Liu, Y. S., Gao, S., Yuan, H. L., Zhao, L., Liu, X. M., Wang, X. C., Hu, Z.C. & Wang, L. S. 2004. U–Pb zircon ages and Nd, Sr, and Pb isotopes of lower crustal xenoliths from North China Craton: insights on evolution of lower continental crust. *Chemical Geology* **211**, 87–109.

Ludwig, K. R. 2005. *Isoplot: A Plotting and Regression Program for Radiogenic Isotope Data, Version 3.23*. Berkeley, California: Berkeley Geochronology Center.

Luo, Z. L., Zhao, X. K., Liu, S. G. & Yong, Z. Q. 2001. Establishment and development of 'Chinese Taphrogeny Outlook'. *Petroleum Geology and Experiment* **23**, 232–41 (in Chinese with English abstract).

Munteanu, M., Yao, Y., Wilson, A. H., Chunnett, G., Luo, Y. N., He, H., Cioaca, M. & Wen, M. L. 2013. Panxi region (South-West China): tectonics, magmatism and metallogenesis. A review. *Tectonophysics* **608**, 51–71.

Peterman, Z. E. & Sims, P. K. 1998. The Goodman swell: A lithospheric flexure caused by crustal loading along the midcontinent rift system. *Tectonics* **7**, 1077–90.

Pierce, K. L. & Morgan, L. A. 2009. Is the track of the Yellowstone hotspot driven by a deep mantle plume? – Review of volcanism, faulting, and uplift in light of new data. *Journal of Volcanology and Geothermal Research* **188**, 1–25.

Qin, J. X., Chen, H. D. & Tian, J, C. 1999. The Permian stratigraphic and paleogeography and their evolution. *Regional Geology of China* **18**, 289–97 (in Chinese with English abstract).

Ren, J. S., Wang, Z. X., Jiang, C. F. & Niu, B. G. 1999. *Chinese Tectonics and its Evolution – 1:5000000 Tectonic Map*. Beijing, China: Geological Publishing House (in Chinese).

Sachau, T. & Koehn, D. 2010. Faulting of the lithosphere during extension and related rift-flank uplift: a numerical study. *International Journal of Earth Sciences* **99**, 1619–32.

Shellnutt, J. G. 2014. The Emeishan large igneous province: a synthesis. *Geoscience Frontiers* **5**, 369–94.

Shellnutt, J. G., Denyszyn, S. & Mundil, R. 2012. Precise age determination of mafic and felsic intrusive rocks from the Permian Emeishan large igneous province (SW China). *Gondwana Research* **22**, 118–26.

Shellnutt, J. G., Usuki, T., Kennedy, A. K. & Chiu, H.-Y. 2015. A lower crust origin of some flood basalts of the Emeishan large igneous province, SW China. *Journal of Asian Earth Sciences* **109**, 74–85.

Sheng, J. & Jin, Y. 1994. Correlation of Permian deposits in China. *Palaeoworld* **4**, 14–113.

Silver, P. G., Behn, M. D., Kelley, K., Schmitz, M. & Savage, B. 2006. Understanding cratonic flood basalts. *Earth and Planetary Science Letters* **245**, 190–201.

Storey, B. C., Alabaster, T. & Pankhurst, R. J. (eds). 1992. *Magmatism and the Causes of Continental Breakup*. The Geological Society of London, Special Publication no. 68.

Sun, Y. D., Lai, X. L., Wignall, P. B., Widdowson, M., Ali, J. R., Jiang, H. S., Wang, W., Yan, C. B., Bond, D. P. G. & Védrine, S. 2010. Dating the onset and nature of the Middle Permian Emeishan large igneous province eruptions in SW China using conodont biostratigraphy and its bearing on mantle plume uplift models. *Lithos* **119**, 20–33.

Ukstins Peate, I. & Bryan, S. E. 2008. Re-evaluating plume-induced uplift in the Emeishan large igneous province. *Nature Geoscience* **1**, 625–9.

Ukstins Peate, I. & Bryan, S. E. 2009. Pre-eruptive uplift in the Emeishan? Reply. *Nature Geoscience* **2**, 531–2.

Ukstins Peate, I., Bryan, S. E., Wignall, P. B., Jerram, D. & Ali, J. R. 2011. Comment on 'Paleokarst on the top of the Maokou Formation: Further evidence for domal crustal uplift prior to the Emeishan flood volcanism'. *Lithos* **125**, 1006–8.

Vauchez, A., Barruol, V. & Tommasi, A. 1997. Why do continents break-up parallel to ancient orogenic belts? *Terra Nova* **9**, 62–6.

Wang, Y., Luo, Z. H., Wu, P., Chen, L. L. & Hao, J. H. 2014. A new interpretation of the sedimentary environment before and during eruption of the Emeishan LIP, southwest China. *International Geology Review* **56**, 1295–313.

Wang, Y., Santosh, M., Luo, Z. H. & Hao, J. H. 2015. Large igneous provinces linked to supercontinent assembly. *Journal of Geodynamics* **85**, 1–10.

White, R. S. & McKenzie, D. P. 1989. Magmatism at rift zones: the generation of volcanic continental margins and flood basalts. *Journal of Geophysical Research* **94**(B6), 7685–729.

Wignall, P. B., Védrine, S., Bond, D. P. G., Wang, W., Lai, X. L., Ali, J. R. & Jiang, H. S. 2009. Facies analysis and sea-level change at the Guadalupian–Lopingian Global Stratotype (Laibin, South China), and its bearing on the end-Guadalupian mass extinction. *Journal of the Geological Society, London* **166**, 655–66.

Xiao, L., He, Q., Pirajno, F., Ni, P. Z., Du, J. X. & Wei, Q. R. 2008. Possible correlation between a mantle plume and the evolution of Paleo-Tethys Jinshajiang Ocean: evidence from a volcanic rifted margin in the Xiaru-Tuoding area, Yunnan, SW China. *Lithos* **100**, 112–26.

Xiao, L., Xu, Y. G., Mei, H. J., Zheng, Y. F., He, B. & Pirajno, F. 2004. Distinct mantle sources of low-Ti and high-Ti basalts from the western Emeishan large igneous provinces, SW China: implications of plume-lithosphere interaction. *Earth and Planetary Science Letters* **228**, 525–46.

Yang, T. N., Hou, Z. Q., Wang, Y., Zhang, H. R. & Wang, Z. L. 2012. Late Paleozoic to Early Mesozoic tectonic evolution of northeast Tibet: evidence from the Triassic composite western Jinsha–Garzê–Litang suture. *Tectonics* **31**, TC4004. doi: 10.1029/2011TC003044.

Zhang, Y. X., Luo, Y. N. & Yang, C. X. 1988. *Panzhihua-Xichang Rift in China*. Series of Geological Memoirs, No. 5. Beijing: Geological Publishing House, 325 pp. (in Chinese).

Zhong, Y. T., He, B., Mundil, R. & Xu, Y. G. 2014. CA-TIMS zircons U-Pb dating of felsic ignimbrite from the Binchuan section: implications for the termination age of Emeishan large igneous province. *Lithos* **204**, 14–19.

Zhou, M. F., Yan, D. P., Kennedy, A. K., Li, Y. & Ding, J. 2002. SHRIMP U–Pb zircon geochronological and geochemical evidence for Neoproterozoic arc-magmatism along the western margin of the Yangtze Block, South China. *Earth and Planetary Science Letters* **196**, 51–67.

Ziegler, P. A. 1992. Geodynamics of rifting. *Tectonophysics* **215**, 221–53.

Ziegler, P. A. & Cloetingh, S. 2004. Dynamic processes controlling evolution of rifted basins. *Earth-Science Reviews* **64**, 1–50.